TECHNICAL ARTICLE

# Cyclic Oxidation and Hot-Corrosion Behavior of HVOF-Sprayed NiCrAl Coating on Industrial Boiler Tube Steels

M.R. RAMESH,[1] SUBBARAO MEDABALIMI,[2] R. SURESH KUMAR,[3] C. DURGA PRASAD ![ORCID],[4,6] and SHRISHAIL B. SOLLAPUR[5]

1.—Department of Mechanical Engineering, National Institute of Technology Karnataka, Surathkal, Mangalore 575025, India. 2.—Department of Mechanical Engineering, SR University, Ananthasagar, Hasanparthy, Warangal Urban, Telangana 506371, India. 3.—Department of Mechanical Engineering, BMS College of Engineering, Bengaluru 560019, Karnataka, India. 4.—Department of Mechanical Engineering, RV Institute of Technology and Management, Bengaluru, Karnataka 560076, India. 5.—Department of IIAEM & ME, Faculty of Engineering and Technology, JAIN (Deemed -to- be University), Bengaluru, Karnataka 560069, India. 6.—e-mail: durgaprasi71@gmail.com

At high temperatures, coatings provide a protective scale development on surfaces to maintain long-term stability. In the current study, ASTM-SA210-Grade A1 (GrA1) and ASTM-SA213-T-11 (T11) boiler tube steels were coated with NiCrAl alloy with high-velocity oxy-fuel (HVOF) to prevent oxidation and hot corrosion. For hot corrosion and oxidation, 50 cycles at 900°C were taken into account. Additionally, tests of hot-corrosion behavior were conducted in an atmosphere containing molten salt ($Na_2SO_4$-60%$V_2O_5$), while tests of oxidation behavior were conducted in static air. The kinetics of oxidation were calculated using the thermogravimetric method. Using XRD, EPMA, and SEM/EDAX methods, the produced oxide scales were characterized. The oxidation rate of NiCrAl-coated steels was found to be lower than that of uncoated steels. The coated steels subjected to oxidation in air exhibit slow scale growth kinetics and oxides of $\alpha$-$Al_2O_3$ and $Cr_2O_3$ on the outermost surface, while accelerated oxidation caused by the molten salt exhibits metastable $Al_2O_3$. Along the nickel-rich splat boundary, Cr and Al were formed a preferential oxidation, which prevents other oxygen from entering the coating via pores and voids, resulting in steady-state oxidation.

## INTRODUCTION

High-temperature resistance to oxidation and corrosion may be achieved by selecting the base material, coating, and deposition method that work well together.[1–3] Most often, ASTM-SA210-Grade A1 (GrA1) and ASTM-SA213-T-11 (T11) are used as base materials in boiler tube applications.[4] These materials must be able to endure a broad range of high-temperature conditions.[5] Ashes produced by residual oil in boiler tubes include a significant quantity of sodium, sulfur, and vanadium, typically as $Na_2SO_4$–$V_2O_5$ and sodium–vanadates combinations. Most of the material mixtures' melting points

are poor (ranging from 100°C to 300°C) and quickly liquefy at boiler operating temperatures (ranging from 600°C to 800°C), causing accelerated corrosion.[6,7] As a result, the base material used in boiler tube applications is made up of iron with molybdenum and chromium as primary additives and with low percentage of carbon, also known as low carbons steels.[8,9] Coatings intended to withstand oxidizing or corrosion conditions at elevated temperatures should produce oxide scales, which are slow growing, thermodynamically stable, and should adhere to the surface.[10] The primary requirements for optimized coatings are that protective phases, such as $Al_2O_3$, $Cr_2O_3$, or $SiO_2$, or spinels of these oxides, should be thermodynamically stable. These protective phases should provide a sufficient reservoir of the oxidizing species to maintain oxide growth over the lifetime of the component.[11] For better surface

protection, the properties of the substrate and coating, like coefficient of thermal expansion, inter-diffusion rate, and protective phases, should be as close to each other as possible.[12] Coatings must also contain sufficient aluminum to produce preferential oxides to have an appropriate reservoir for restoring the protective oxide when removed.[13]

Mahesh et al.[14] deposited a NiCrAl coating by the high velocity oxy-fuel (HVOF) process on Fe- and Ni-based superalloys. After 10 oxidation cycles at 700°C, oxide phases like $Al_2O_3$, $NiO$, and $Cr_2O_3$ were developed on the surface. Each cycle consisted of heating for 100 h at 700°C and 1 h cooling. After subjecting the coated specimens to repeated exposure in a coal-fired boiler atmosphere at 700°C for 1000 h, a notably thin oxide layer was detected. This partially oxidized coating intimately adhered to the underlying substrate. The presence of aluminum and chromium oxides, formed alongside the nickel-rich splat boundaries, acted as a barrier, impeding the continued diffusion of corrosive elements into the coating and, consequently, into the substrate alloy. Singh et al.[15] used HVOF-sprayed NiCrAlY coating deposited on a T-91 substrate. After 50 cycles of oxidation at 900°C, with each cycle including heating for 1 h 20 min cooling with total of 45,000 h of cyclic heating, protective oxides like $Al_2O_3$, $NiO$, $Cr_2O_3$, and $CrO$ were produced. CrN, AlCrN, and TiAlN coatings were applied on Waspaloy base material using the arc evaporation physical vapor deposition procedure, and its behavior at high temperatures was evaluated by Biava et al.[16] Scholars have also examined the oxidation and hot-corrosion behaviors of preceramic-based dual-layer coatings based on plasma electrolytic oxidation and plasma electrolytic oxidation /polysilazane, twin wire arc-sprayed and HVOF NiCr-based coatings, and high-velocity arc-sprayed Ni-Cr alloy coatings.[17–32] Traditional methods such as flame spraying failed in the past, but in recent years plasma spraying and the HVOF process have made significant progress.[33–40] Compared to other thermal spray processes, the HVOF process produces a high-quality coating with a homogeneous and dense structure.[41–50] Several studies are being conducted to investigate the various coating deposition possibilities with the HVOF process on multiple materials. Thick and microstructurally homogeneous coatings are needed to achieve high corrosion resistance on the surfaces.[51–60] Hence, the combination of GrA1 and T11 base material were selected to deposit NiCrAl coatings by the HVOF process to test the performance of oxidation and hot corrosion at high temperature.

This paper's main objective is to study the cyclic oxidation (in static air) and hot corrosion (in molten salt $Na_2SO_4$-60%$V_2O_5$) behavior of NiCrAl coatings deposited by the HVOF process on GrA1 and T11 steels at 900°C. Cyclic experiments were conducted to address the issue of metal corrosion at cyclic temperatures rather than isothermal temperatures.

## MATERIALS AND METHODS

### Deposition of Coating

T11 and GrA1 are low-carbon steels used as substrate materials. These steels are used in coal-fired thermal power plants as superheaters and re-heater tubes. The elemental composition of these steels, as determined by spectroscopy, is shown in Table I. The substrates were cut previously from the cross-sections of boiler tubes and the curved surface developed into a flat surface without affecting the base material properties. The flat plate was grit-blasted on both sides with alumina particles. The wire-cut electrical discharge machining process was used to cut the substrate from the flat plate to the required dimensions (20 mm × 15 mm × 5 mm).

The substrates were polished with a motor-driven 180-grit emery paper. The specimen surfaces were grit-blasted with $Al_2O_3$ (grit size 45) and the coating deposited on them. The HVOF technique (HIPOJET 2100) was used to deposit NiCrAl coatings on all the substrate surfaces. The process parameters for HVOF spraying are shown in Table II. In this analysis, commonly produced NiCrAl powder (MEC-1047) with the composition Ni-17.92Cr-6.66Al (wt.%) was used in this study.

### Characterization of as-Sprayed Coatings

The porosity of the coating is an important factor in hot-corrosion investigations. The porosity study was carried out using image analysis tools. To assess the porosity, 20 separate images were examined at a magnification of × 250 for each sample. The coating densities were calculated using the water immersion technique under ASTM C-135-96. Using a load of 300 g and a dwell time of 10 s over the coating–substrate contact, a Vickers microhardness tester (MVH-S-AUTO) was used to obtain the microhardness values. Scanning electron microscopy/energy dispersive spectroscopy (SEM/EDS) and X-ray diffraction (XRD; DXGE−2P; Jeol, Japan) studies were used to examine the surface and cross-sectional morphologies of the as-sprayed coatings.[61–65]

### Cyclic Oxidation and Hot Corrosion

Both coated and uncoated samples were used for testing the cyclic oxidation and hot corrosion. Throughout all 50 cycles, an aggregate of six samples was employed for testing: three samples from the coated group and three from the uncoated group. The recorded results represent the average outcomes obtained from three samples. Each cycle involved heating the samples to 900°C and processing them in the furnace for 1 h. After removing the heated samples from the furnace, they were allowed to cool in the open air for 20 min. The samples' weights were recorded, and visual measurements were taken to better understand the oxide scale's physical aspects that evolved during each cycle.[66–71]

**Table I. Chemical composition (wt.%) of boiler tube steels**

| Type of steel | C | Mn | Si | S | P | Cr | Mo | Fe |
|---|---|---|---|---|---|---|---|---|
| GrA1 | 0.2471 | 0.5649 | 0.2314 | 0.0049 | 0.0104 | - | - | Bal. |
| T11 | 0.1361 | 0.5102 | 0.4852 | 0.0073 | 0.0159 | 1.1067 | 0.5204 | Bal. |

**Table II. Process parameters of HVOF spraying**

| Air pressure | 588 kPa |
|---|---|
| Air-flow rate | 700 l/min |
| Fuel (LPG) pressure | 588 kPa |
| Fuel flow rate | 60 l/min |
| Oxygen pressure | 883 kPa |
| Oxygen flow rate | 250 l/min |
| Powder feed rate | 38 g/min |
| Spray distance | 200 mm |

The samples were subjected to heating using a tubular furnace (Heatron Industrial Heaters, India). Initially, for the first cycle, the samples were placed in the furnace once it reached a temperature of 900°C. Subsequently, for the following cycles, the furnace operation continued uninterrupted, while the samples were taken out and the furnace was sealed using glass wool insulation to sustain a consistent temperature without stopping the furnace operation.

Similarly for the hot-corrosion studies, 50 cycles were considered with six samples, three from each coated and uncoated group. The results represent the average outcomes obtained from three samples. The samples were covered with a semisolid-state salt ($Na_2SO_4$-60%$V_2O_5$) dissolved in distilled water in the range of 3.0–5.0 mg/cm$^2$. Between cycles, the samples affected by corrosion were not cleaned; instead, they were consistently maintained within a ceramic boat designed to collect any accumulated oxide scales that might have detached from the samples. In order to better understand the corrosion kinetics, weight transition values were determined at the end of each cycle. The samples were subjected to SEM and XRD after oxidation and hot-corrosion tests to obtain information about the formed phases and their structure on the surfaces. The XRD analysis was conducted operating at 40 kV and 40 mA. Cu-K$\alpha$ radiation with a wavelength of $\lambda = 0.154$ nm was used for the analysis. The XRD patterns were scanned over the range of 10–100°, employing a step size of 0.02°.

## RESULTS

### Characterization of as-Sprayed Coatings

HVOF-sprayed NiCrAl coatings on both substrates have an average coating thickness of 260 μm. Three trials were performed to measure the mean value of the coating thickness which had a
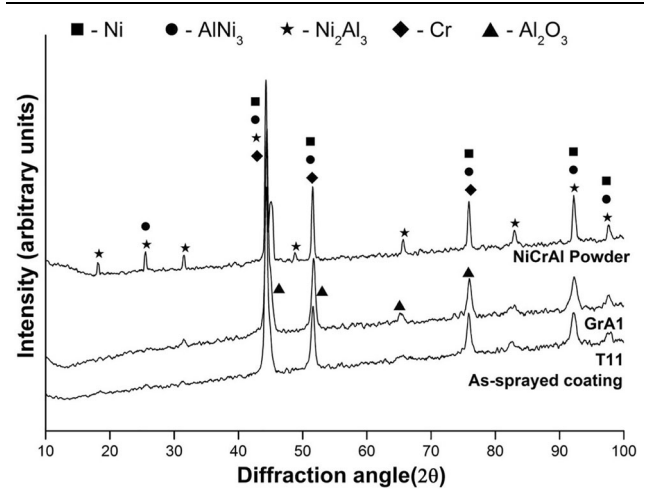


Fig. 1. X-ray diffraction patterns of NiCrAl powder and as-sprayed coating on GrA1 and T11 substrates.

range of 250–275 μm. The coatings were found to have a less than 1% porosity value, and the average microhardness value measured over the coating was $366 \pm 15$ HV$_{0.3}$. The coating's average density was found to be $3.05 \pm 0.32$ g/cm$^3$ when analyzed using the water immersion process. Powder and as-sprayed coatings on the GrA1 and T11 substrates were analyzed using XRD (Fig. 1). Compared to the powder, the NiCrAl coating on both substrates has similar peaks, indicating that the phase structure after spraying has not changed significantly. The XRD patterns of the powder and coating showed one common main phase of nickel-rich FCC structure. The presence of weak $Al_2O_3$ intensity peaks indicates that there was just a minor amount of oxidation during spraying. Figure 2 depicts the EDS of melted and partially melted particles of the as-sprayed NiCrAl coating. The surface shows the overlaying of separate splats as globules of partly melted particles scattered throughout a molten matrix. The partly melted particles were discovered to have a significant concentration of nickel. The weight percentage of elements present in the alloy powders were 75.42%Ni-17.92%Cr-6.66%Al, which shows that partially melted particles are closer to the original composition of the powder particles.

### Thermocyclic Oxidation in Air and Salt

The amount of weight gained by hot corrosion in a molten salt environment is more significant than the amount of weight gained by oxidation in an air
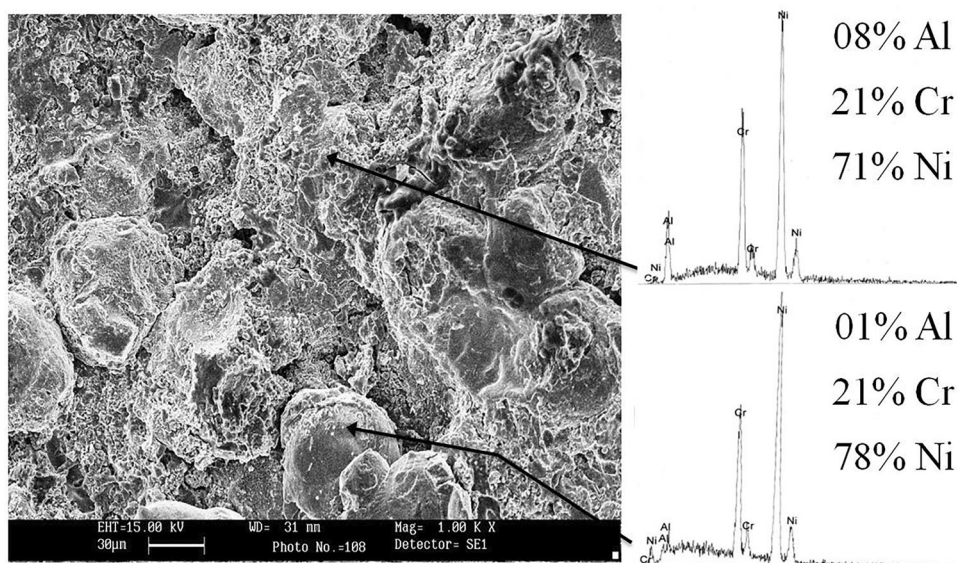
Fig. 2. Surface morphology of as-sprayed NiCrAl coating showing elemental composition at melted and partially melted particles on the surface.
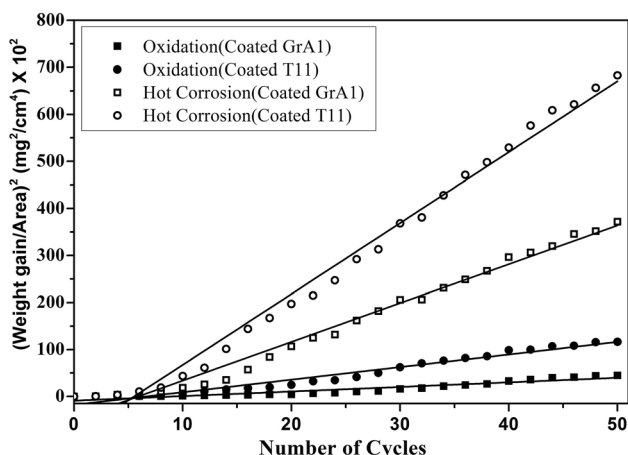


Fig. 3. Square of weight gained/area versus number of cycles plot for NiCrAl-coated steels of cyclic oxidation and hot corrosion, and each cycle included heating the sample to 900°C for 1 h followed by air-cooling for 0.3 h to measure the weight gained.
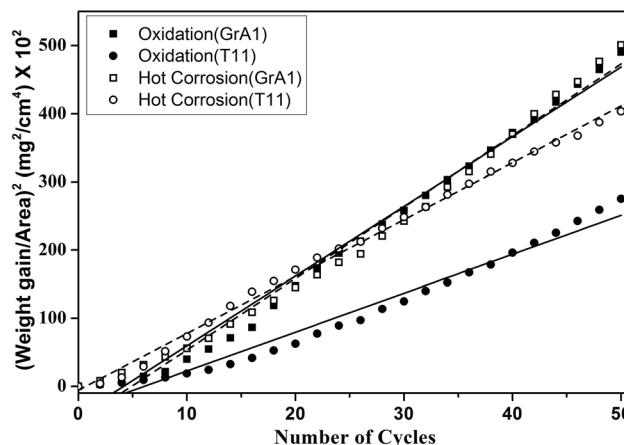


Fig. 4. Square of weight gained/area versus number of cycles plot for uncoated steels of cyclic oxidation and hot corrosion, and each cycle included heating the sample to 900°C for 1 h followed by air-cooling for 0.3 h to measure the weight gained.

environment. Up to 50 cycles, the oxidation behavior of the coatings in air and salt can be assumed to be parabolic (Fig. 3). A linear least-squares fit method has been used to measure the parabolic rate constant Kp ($10^{-8}$ $g^2$ $cm^{-4}$ $s^{-1}$). The $K_p$ values for NiCrAl-coated GrA1 and T11 steels exposed to oxidizing in the presence of air are $0.027 \times 10^{-8}$ $g^2$ $cm^{-4}$ $s^{-1}$ and $0.075 \times 10^{-8}$ $g^2$ $cm^{-4}$ $s^{-1}$, and in molten salt, are $0.229 \times 10^{-8}$ $g^2$ $cm^{-4}$ $s^{-1}$ and $0.419 \times 10^{-8}$ $g^2$ $cm^{-4}$ $s^{-1}$, respectively. During the hot corrosion tests, the T11 steel showed the most significant increase of weight. The value of T11 is more than twice the weight gain of the GrA1 steel oxidized in air at the same temperature. The observable deviation from the parabolic rate for uncoated steels (Fig. 4) indicates that the oxide layers were only marginally effective at 900°C. The

GrA1 steel appears to have the maximum weight gain, but the scale formed was brittle and suffered severe oxide scale spalling.

## XRD Analysis

Figure 5 shows the NiCrAl-coated steel's XRD patterns after 50 cycles of oxidation, which revealed phases like $\alpha$-$Al_2O_3$, Ni, $AlNi_3$, and mixed spinel-type oxide, $NiCr_2O_4$. In the molten salt environment, the XRD pattern shows (Fig. 6) the significant phases of $\delta$-$Al_2O_3$, $\theta$-$Al_2O_3$, NiO, $Cr_2O_3$, $NiCr_2O_4$, and $NiAl_2O_4$ along with minor phases of $Ni_3V_2O_8$, $AlVO_4$, and $CrVO_4$.

## Structure and Composition of Oxide Scale

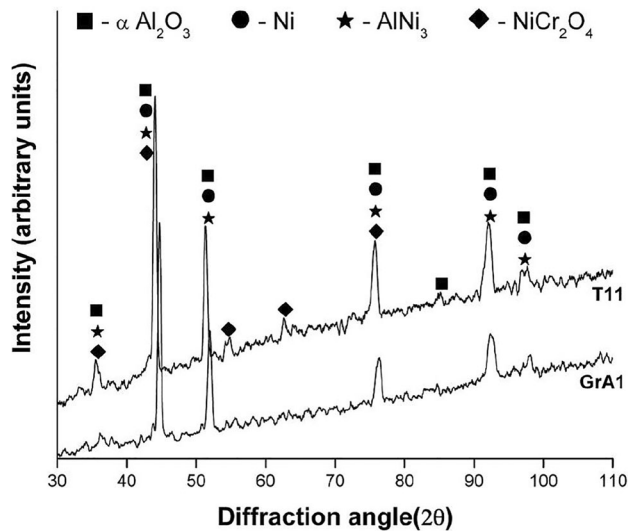Figure 7a shows different morphologies of the oxide scale of NiCrAl-coated GrA1 steel. The

Fig. 5. XRD patterns of NiCrAl-coated steels after 50 oxidation cycles, each cycle including heating the sample to 900°C for 1 h followed by air-cooling for 0.3 h to measure the weight gained.
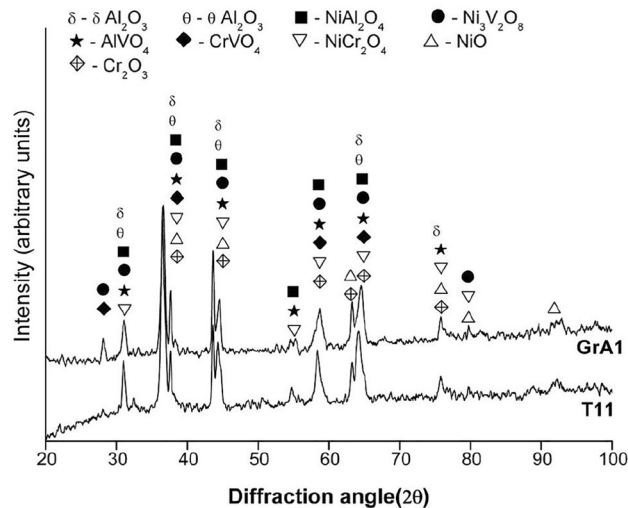


Fig. 6. XRD patterns of NiCrAl-coated steels after 50 cycles of hot-corrosion testing, each cycle including heating the sample to 900°C for 1 h followed by air-cooling for 0.3 h to measure the weight gained.

energy-dispersive X-ray spectroscopy (EDAX) examination of spherical globules on the surface reveals a higher concentration of Ni and Cr oxides, while the matrix reveals a higher concentration of O and Al. Figure 7b shows the oxide scale of corroded NiCrAl-coated steel, which had a blade-like surface with smooth patches containing higher O and Al. The blade-like structure could correspond to $\theta$-$Al_2O_3$. The polyhedral crystals on the oxide scale have a relatively higher amount of $Cr_2O_3$ and NiO. Minor amounts of $V_2O_5$ and $Na_2O$ are also indicated on the surface of the oxide scale.

The composition of the NiCrAl-coated T11 steel (Fig. 8a) after 50 cycles of oxidation indicates that the scale's outermost layer mainly consists of Ni, Al, and Cr oxides. Points 2 and 5 in the figure indicate Ni- and Cr-rich splat without oxidization. Cr, Al, and O concentrations are high at points 3 and 6, revealing internal oxidation along the splat boundary. The dark phase found at the contact between the coating and the substrate is high in Al and O (point 7), suggesting that it is a remnant of the surface preparation before HVOF spraying. A persistent and adherent thick layer of scale has been found on the top of the coating after 50 cycles of hot corrosion (Fig. 8b). The thickness of this outermost oxide layer, as measured from the back-scattered electron image, is in the range of 25–50 $\mu$m containing Ni and Cr along with a lower percentage of Al (points 1 and 2). The white grains (point 3) underneath the uppermost oxide layer correspond to the nickel-rich splats in an unoxidized state, whereas internal oxidation has occurred along the splat boundary. The presence of a minor amount of iron at the contact between the coating and the substrate (point 5) explains how the iron diffused into the coating.

### Electron Probe Micro-Analysis (EPMA)

Figure 9 depicts X-ray elemental mapping along the cross-section of NiCrAl-coated T11 steel after cyclic oxidation, and each cycle included heating the sample to 900°C for 1 h followed by air-cooling for 0.3 h to measure the weight gained. The steel shows a thin adherent layer of oxide scale rich in protective $Al_2O_3$ oxide scale. The mapping also reveals that Al and Cr are selectively oxidized along the splat boundary, while nickel-rich splats are unoxidized. The arrow indicates a slight diffusion of substrate iron into the coating via open pores available at the splat boundary, which aids in better bonding.

Figure 10 depicts X-ray elemental mapping along the cross-section of the NiCrAl-coated GrA1 steel after cyclic hot corrosion, and each cycle included heating the sample to 900°C for 1 h followed by air-cooling for 0.3 h to measure the weight gained. Corroded NiCrAl-coated GrA1 steel depicts the formation of a thick uppermost oxide layer consisting primarily of Ni and Cr oxides. This oxide scale also has several patches of aluminum oxides. During the hot corrosion for 50 cycles, the higher V and Na concentrations are limited to the surface and do not penetrate deeply into the coating.

### DISCUSSION

Thick coatings shows longer life times;[25] however, the width of thicker coatings is limited due to self-disintegration. Higher coating thickness may result in cracks between the splats boundaries because of residual stresses formed during the solidification of the deposited coating. The average thickness of coatings obtained using the HVOF process is 260 $\mu$m, which is well within the acceptable range of 250 $\mu$m–300 $\mu$m as recommend by Sidhu.[26] and

| 07 O | 03% O |
| 26% Ni | 32% Ni |
| 38% Cr | 50% Cr |
| 29% Al | 15% Al |

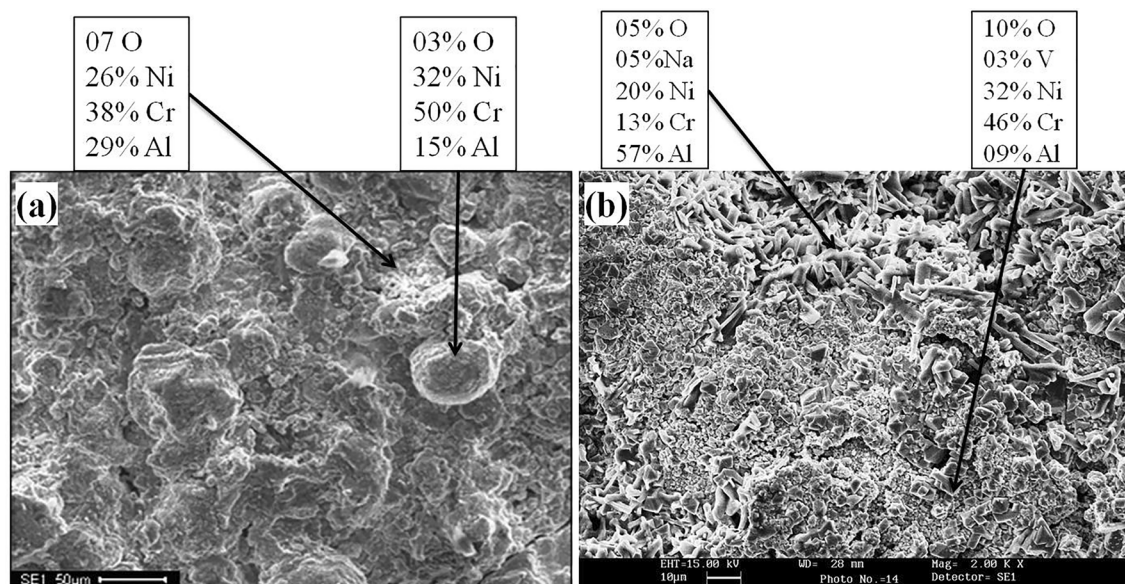| 05% O | 10% O |
| 05% Na | 03% V |
| 20% Ni | 32% Ni |
| 13% Cr | 46% Cr |
| 57% Al | 09% Al |

Fig. 7. SEM and EDAX point analysis of NiCrAl-coated GrA1 steel subjected to cyclic (a) oxidation and (b) hot corrosion, and each cycle including heating the sample to 900°C for 1 h followed by air-cooling for 0.3 h to measure the weight gained.

Nicholls[27] Higher kinetic energy and melting behavior of powder particles during HVOF spraying contribute to lower porosity values. When partially melted powder particles (Fig. 2) hit the substrate at high velocity, they develop an almost porosity-free coating. For HVOF-sprayed nickel chrome coatings, the measured porosity values correlated with the findings of Sahroui et al.,[28] Sidhu et al.,[29] and Miguel et al.[30] Because of the sprayed particles' supersonic speeds, they only had a short exposure to an oxidizing atmosphere, resulting in mild heating. Thus, the XRD peaks of the as-sprayed coating and powder particles are almost identical.

### Cyclic Oxidation in Air

The NiCrAl-coated steels had slightly lower weight gain values than the uncoated steels, 1/33 and 1/15 of the uncoated GrA1 and T11 steel substrates, respectively. The oxidation behavior of the coated steels shows a parabolic curve up to 50 cycles, and the formed oxide scales on the surface act as diffusion barriers to the oxygen. The parabolic rate constants (Kp) for all the coated steels exhibit a consistent trend of being lower compared to the uncoated steels. This trend strongly suggests that the coated steels experience slower oxidation rates. The oxidation behavior observed in the coated steels follows a parabolic pattern throughout the 50 cycles, indicating that the formed oxide scales tend to function as effective diffusion barriers. These findings align with those reported by Sidhu et al.,[29] who demonstrated improved oxidation resistance in plasma-sprayed NiCrAlY coatings compared to a boiler steel substrate oxidized in air at 900°C.

$\alpha$-Al$_2$O$_3$ is a significant phase on the oxidized surface (Fig. 5). $\alpha$-Al$_2$O$_3$ is the thermodynamically stable phase, which avoid the oxide scale growth.[31]

Further, EDAX (Fig. 8a) and EPMA (Fig. 9) analyses confirmed the presence of a thin layer of Al$_2$O$_3$ along with Cr and Ni oxides. Spinel oxide phase NiCr$_2$O$_4$ may result from initially grown NiO and Cr$_2$O$_3$. Due to the restriction of Al diffusivity, the AlNi$_3$ phase may have segregated during the oxidation process. Thus, Al diffusivity promotes the formation of a continuous $\alpha$-Al$_2$O$_3$ by holding a more considerable amount of Al and slowing down the reaction. NiO and $\alpha$-Al$_2$O$_3$ could have gone through a solid-state reaction to form NiAl$_2$O$_4$ during the initial oxidation period. However, an increase in oxidation time and transformation, results in thermally stable $\alpha$-Al$_2$O$_3$, and spinel oxide NiAl$_2$O$_4$ could have been overlaid by the growing Al$_2$O$_3$. This is supported by Chen et al.[32] findings from their research on the oxidation behavior of sputtered NiCrAl nanocrystalline coatings.

The nickel-rich splat border is where preferential oxides of Al and Cr were produced.[33] The selective oxidation of HVOF coatings is controlled by many factors, such as the flattened structure, affinity for oxygen, and the free energy of oxide generation. Aluminum oxidizes before Cr ($\Delta G° = -813.85$ kJ mol$^{-1}$) and Ni ($\Delta G° = -132.31$ kJ mol$^{-1}$) because of its very negative free energy of oxide production ($\Delta G° = -1295.66$ kJ mol$^{-1}$ at 925°C).[33] First, oxygen enters the coatings via the open porosity around the splat borders. This causes Al and Cr to partially oxidize, which stops more oxygen from entering the coating. Consequently, the exterior coating surface is where subsequent oxidation mostly takes place. The observed decreased thickness of the oxide scale in this study may be attributed to the inhibition of additional oxide formation caused by the oxidation of aluminum into
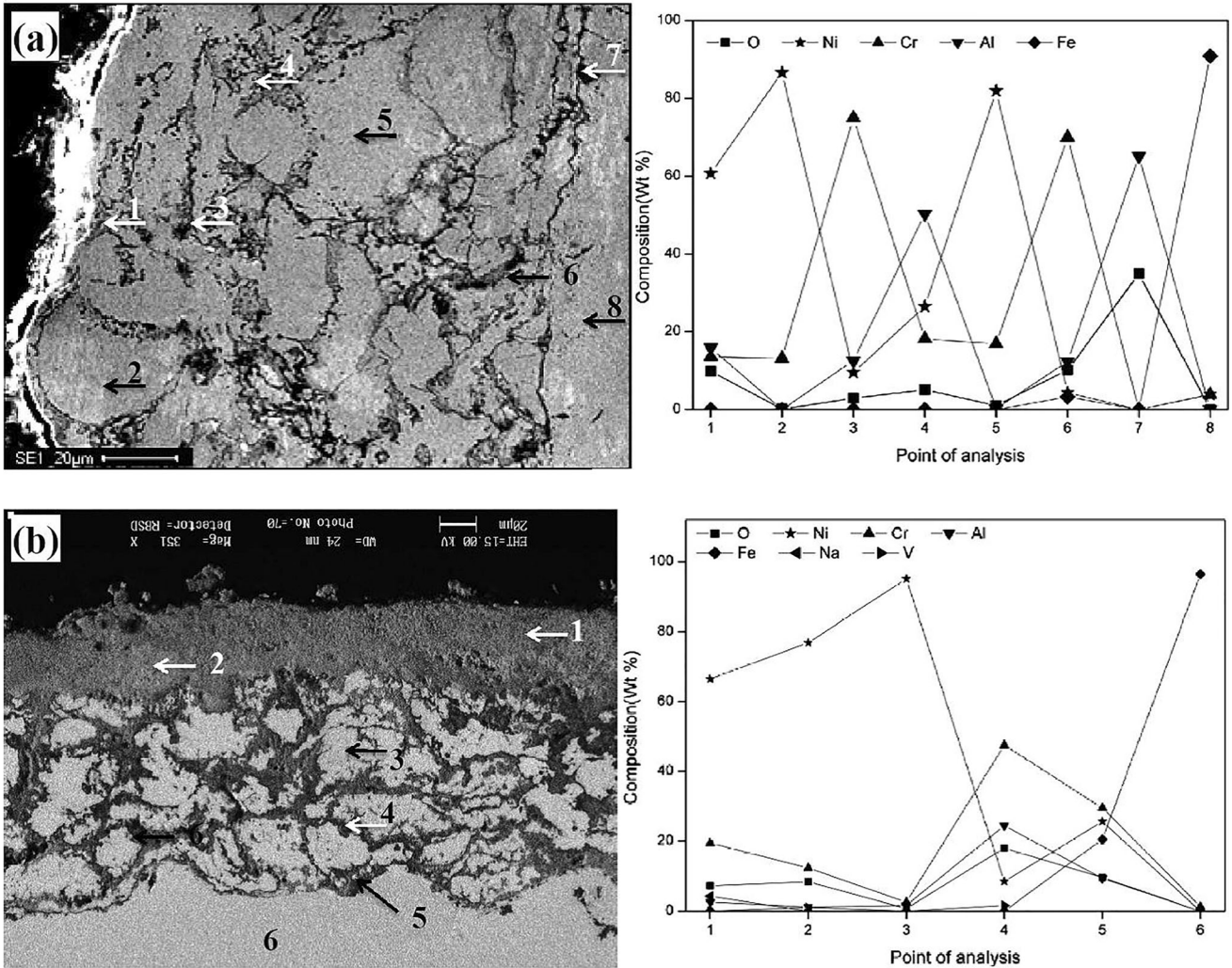
Fig. 8. BSEI and composition analysis across the cross-section of NiCrAl-coated T11 steels subjected to cyclic (a) oxidation and (b) hot corrosion, each cycle including heating the sample to 900°C for 1 h followed by air-cooling for 0.3 h to measure the weight gained.

$\alpha$-$Al_2O_3$. Similar observations of internal oxidation via open pores during the early stages of oxidation for thermal-sprayed MCrAlY coatings have been reported by Sidhu and Prakash,[5] Singh et al,[34] and Niranatlumpon et al.[35]

The preceding explanation is represented by the following equations. The creation of $\alpha$-$Al_2O_3$ scale on the alloy surface requires suitable thermodynamic conditions for:[36]

$$2Al + 3/2\ O_2 \rightarrow Al_2O_3$$
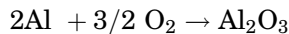
Because of the initial oxygen supply, reactions of this kind also generate other oxides besides $Al_2O_3$:

$$M + 1/2\ O_2 \rightarrow MO$$
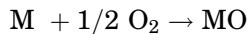
where M stands for additional metallic parts. In order for the $Al_2O_3$ to form a continuous scale, there has to be a positive extra reaction:

$$2Al + 3MO \rightarrow Al_2O_3 + 3M$$
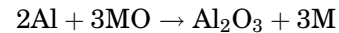
Generally, behind a portion of the MO layer, the $Al_2O_3$ becomes continuous. As the coating continues to oxidize and suffers from a significant Al depletion, it will be advantageous for the formation of additional oxides and spinel:

$$Al_2O_3 + 2Cr \rightarrow 2Al + Cr_2O_3 \text{or} Al_2O_3 + 1/2O_2 + Ni \rightarrow NiAl_2O_4$$
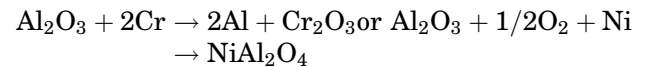
Additionally, in the NiO that was generated during the first oxidation, Cr atoms replace Ni atoms, generating a significant quantity of $Cr_2O_3$:

$$3NiO + 2\ Cr \rightarrow 3\ Ni + Cr_2O_3$$
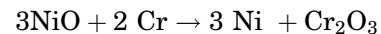
In addition to interacting with alumina to produce $NiAl_2O_4$, this nickel may have also interacted with aluminum and carbon to produce spinels:
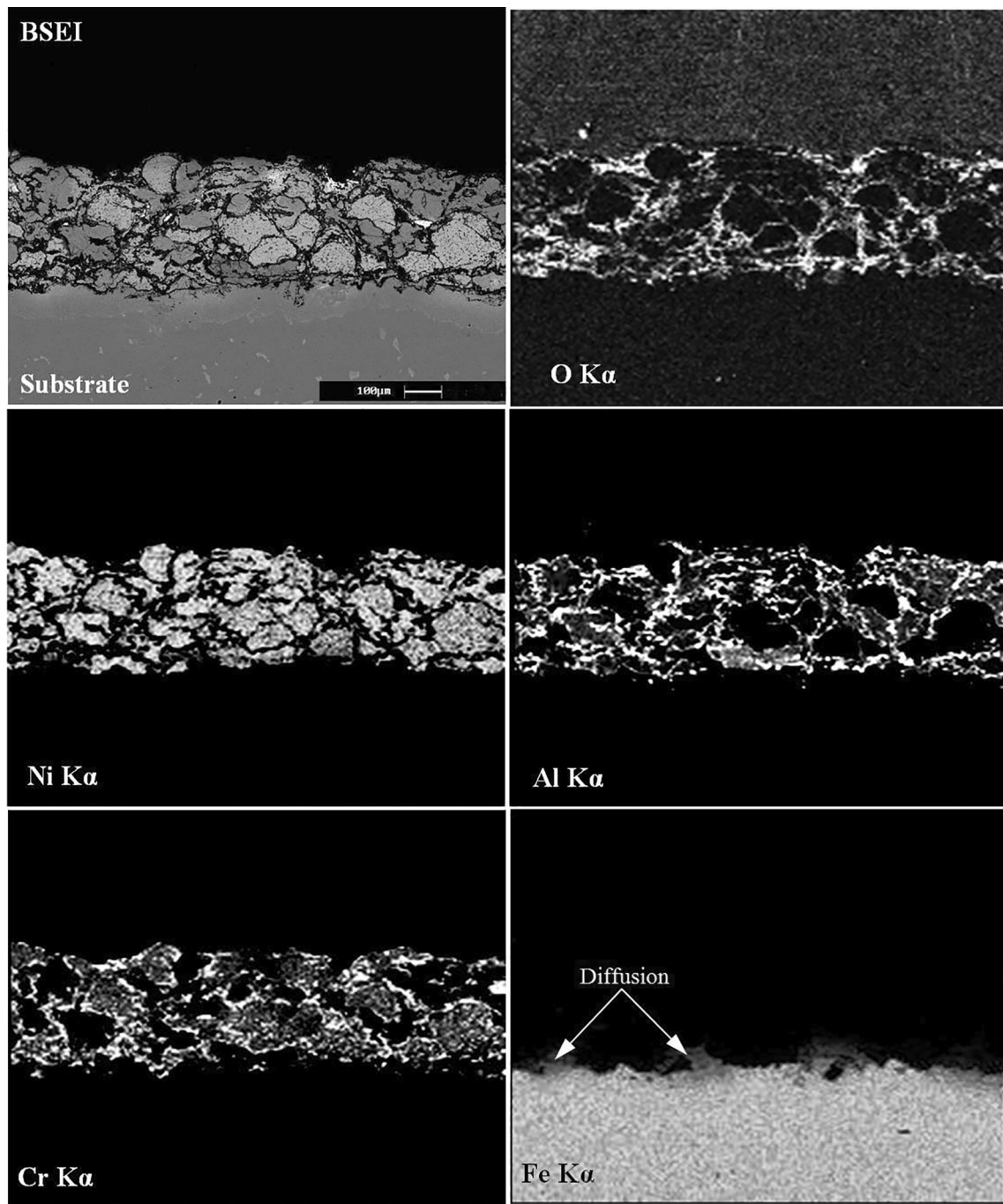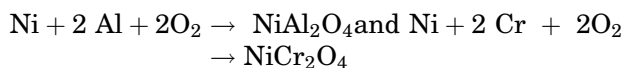
Fig. 9. X-ray elemental mapping along the cross-section of NiCrAl-coated T11 steel after cyclic oxidation, each cycle including heating the sample to 900°C for 1 h followed by air-cooling for 0.3 h to measure the weight gained.

$$Ni + 2\,Al + 2O_2 \rightarrow NiAl_2O_4 \text{ and } Ni + 2\,Cr + 2O_2 \rightarrow NiCr_2O_4$$

**Hot Corrosion**

The NiCrAl-coated steels exhibit notably lower weight gain compared to their uncoated counterparts when subjected to a $Na_2SO_4$-60%$V_2O_5$ molten salt environment. After 50 cycles of exposure, the weight gain of NiCrAl-coated GrA1 and T11 steels is, respectively, 1/11 and 1/7 times that of the uncoated steels of the same type. Additionally, the parabolic rate constant (Kp) displays a consistent decrease across all the coated steels compared to the uncoated steels. This suggests that the HVOF-sprayed NiCrAl coatings effectively provide the necessary protection to the substrate steels. Similar conclusions have been drawn in studies by Sidhu
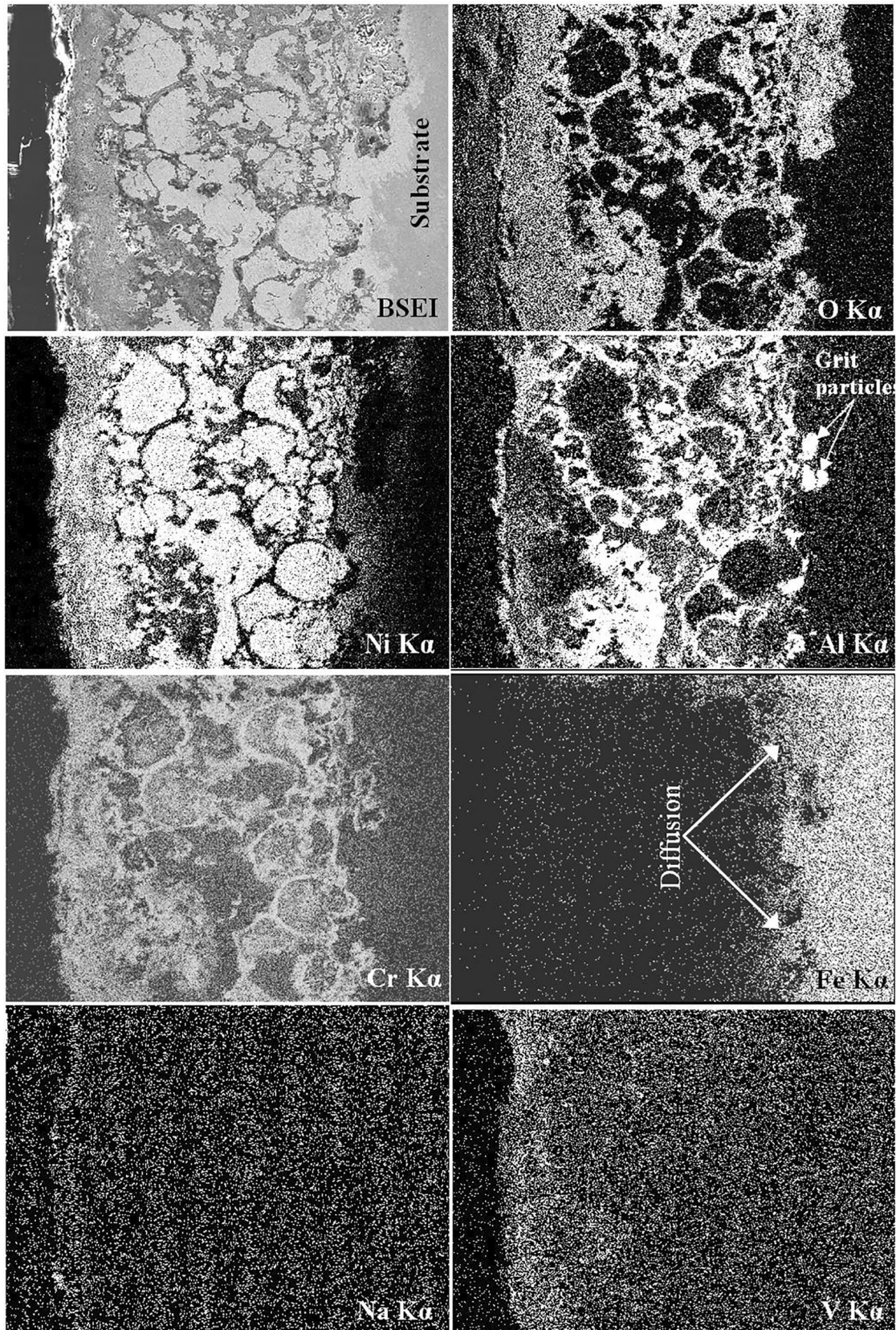
Fig. 10. X-ray elemental mapping along the cross-section of NiCrAl-coated GrA1 steel after cyclic hot corrosion, each cycle including heating the sample to 900°C for 1 h followed by air-cooling for 0.3 h to measure the weight gained.
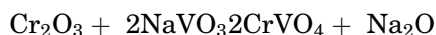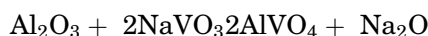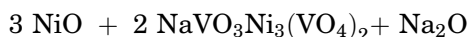
et al.[29] and Singh et al.,[34] demonstrating superior corrosion resistance of plasma-sprayed NiCrAlY coatings in comparison to substrate boiler steels and Fe-based superalloys exposed to $Na_2SO_4$ -60%$V_2O_5$ environments at 900°C.

A continuous and thick compact layer of scale is formed on the top of the corroded coating containing phases of $\delta$-$Al_2O_3$, $\theta$-$Al_2O_3$, NiO, $Cr_2O_3$, $NiCr_2O_4$, and $NiAl_2O_4$, and traces of $Ni_3V_2O_8$, $AlVO_4$, and $CrVO_4$. The $\theta$-$Al_2O_3$ exists a blade-like structure in smooth patches. It is expected that the metastable $Al_2O_3$ was formed in the initial cycles caused by accelerated oxidation. Similar results were reported by Brandl et al.[37] with a MCrAlY coating and Guofeng et al.[32] with a NiCrAl nanocrystalline coating that the metastable $Al_2O_3$ was formed during the oxidation of HVOF-sprayed coatings. Further, NiO and spinel oxides prevent the exclusive development of $Cr_2O_3$ layer, although the Cr concentration is 17.92% in the coating. Further, NiO and spinel oxide phases prevent the exclusive development of a $Cr_2O_3$ layer, even though the Cr concentration is more than 13% in the coating. The acidic dissolution reactions may have resulted in the initially developed oxide layer's degradation on the coating surface.[38–42] The preferential oxidation of Al and Cr along the nickel-rich splats boundaries acts as a diffusion barrier to the corrosive species' inward diffusion.[43–46]

The results from EPMA and EDAX show where Na and V are distributed in the highest oxide scale. This distribution points to the possibility of an acidic fluxing caused by the combination of $Na_2SO_4$ -60%$V_2O_5$. According to existing thermodynamic data, $Na_2SO_4$ has the capability to react with $V_2O_5$, leading to an increase in the melt's acidity through the formation of vanadates, specifically $NaVO_3$, as described by the following reaction at 900°C:[38]

$$Na_2SO_4 + V_2O_5 \rightarrow 2NaVO_3 + SO_2 + \tfrac{1}{2}O_2$$

NiO, $Al_2O_3$, and $Cr_2O_3$ dissolve acidically when this NaVO3 serves as a catalyst, and, based on the reactions, this is most likely what happened:[40]

$$3\,NiO + 2\,NaVO_3 Ni_3(VO_4)_2 + Na_2O$$

$$Al_2O_3 + 2NaVO_3 2AlVO_4 + Na_2O$$

$$Cr_2O_3 + 2NaVO_3 2CrVO_4 + Na_2O$$

The originally created oxide layer on the coated surface could have broken down as a result of these dissolving events. The XRD and EPMA data also support the production of such metal vanadates, which are primarily located on the top scale.

The EPMA study showed that Al and Cr underwent preferential oxidation at the nickel-rich splat borders, which served as an efficient barrier to prevent corrosive ions from diffusing inside. The nickel-rich splats themselves, interestingly enough, did not oxidize during the course of the 50 cycles of the high-temperature corrosion experiments. Analysis of the coating–substrate interface revealed a reciprocal diffusion process wherein iron diffused into the coating, and components from the coating, such Ni, Cr, and Al, diffused into the substrate to improve the binding between the layers. Moreover, grit particles at the coating–substrate contact are evidence of surface preparation left behind from the HVOF spraying procedure.

## CONCLUSION

- GrA1 and T11 boiler tube steels had NiCrAl alloy coatings applied to them with success using HVOF thermal spraying. With the specified spray conditions, an apparently dense laminar-structured coating with a porosity of less than 1% and an average thickness of 260 $\mu$m was obtained.
- XRD patterns of the as-sprayed coatings show almost equivalent peaks to those of the powder, demonstrating a negligible difference in phase structure after spraying.
- Compared to the uncoated steels, the lower parabolic rate constant ($K_p$) of NiCrAl coatings proves lower oxide rates of the coated steels. The uncoated steels experience intense spalling and peeling of oxide scale from the surface.
- The NiCrAl coatings' protection subjected to oxidation in the air can be attributed to the oxide layer of $\alpha$-$Al_2O_3$ and $Cr_2O_3$ formed on the outermost surface. $\alpha$-$Al_2O_3$ is a thermodynamically stable phase having a close-packed corundum structure. Due to the restriction of Al diffusivity, the $AlNi_3$ phase may have segregated during the oxidation process. Thus, Al diffusivity promotes the formation of a continuous $\alpha$-$Al_2O_3$ by holding a more considerable amount of Al and slowing down the reaction.
- In conditions with molten salt, NiCrAl-coated steels showed a strong protective oxide layer made of Ni and Cr oxides which resists hot corrosion..
- Early oxidation stages prevent oxygen and corrosion species from penetrating the coating by preferentially oxidizing Al and Cr along the nickel-rich splat border. This allows the oxidation rate to stabilize.

## FUNDING

## DATA AVAILABILITY

Not applicable

## CONFLICT OF INTEREST

The authors declare there are no conflicts of interest.

## REFERENCES

1. P.S. Sidky and M.G. Hocking, Review of inorganic coatings and coating processes for reducing wear and corrosion. *Br. Corros. J.* 34, 171 https://doi.org/10.1179/000705999101500815 (1999).

2. J. Stringer, Role of coatings in energy-producing systems: an overview. *Mater. Sci. Eng.* 87, 1 https://doi.org/10.1016/0025-5416(87)90355-7 (1987).

3. T.S. Sidhu, S. Prakash, and R.D. Agrawal, A comparative study of hot corrosion resistance of HVOF sprayed NiCrBSi and Stellite-6 coated Ni-based superalloy at 900°C. *Mater. Sci. Eng.* 446, 210 https://doi.org/10.1016/j.msea.2006.09.015 (2007).

4. B.S. Sidhu, D. Puri, and S. Prakash, Characterisations of plasma sprayed and laser remelted NiCrAlY bond coats and Ni3Al coatings on boiler tube steels. *Mater. Sci. Eng. A* 368(1–2), 149 https://doi.org/10.1016/j.msea.2003.10.281 (2004).

5. B.S. Sidhu and S. Prakash, Degradation behavior of Ni3Al plasma-sprayed boiler tube steels in an energy generation system. *J. Mater. Eng. Perform.* 14, 356 https://doi.org/10.1361/10599490523382 (2005).

6. R. Bhatia, H. Singh, and B.S. Sidhu, Hot corrosion studies of HVOF-sprayed coating on T-91 boiler tube steel at different operating temperatures. *J. Mater. Eng. Perform.* 23, 493 https://doi.org/10.1007/s11665-013-0771-0 (2014).

7. S.T. Bluni and A.R. Marder, Effects of thermal spray coating composition and microstructure on coating response and substrate protection at high temperatures. *Corros.* 52, 213 https://doi.org/10.5006/1.3292116 (1996).

8. R. Kumar, V.K. Tewari, and S. Prakash, Studies on hot corrosion of the microstructurally different regions of 225 Cr-1Mo (T22) boiler tube steel weldment. *J. Mater. Eng. Perform.* 18, 959 https://doi.org/10.1007/s11665-008-9309-2 (2009).

9. J.N. Harb and E.E. Smith, Fireside corrosion in pc-fired boilers. *Prog. Energy Combust. Sci.* 16, 169 https://doi.org/10.1016/0360-1285(90)90048-8 (1990).

10. H. Singh, S. Prakash, D. Puri, and D.M. Phase, Cyclic oxidation behavior of some plasma-sprayed coatings in Na 2so4-60%V2O5 environment. *J. Mater. Eng. Perform.* 15, 729 https://doi.org/10.1361/105994906X150858 (2006).

11. L. Ahuja, D. Mudgal, S. Singh, and S. Prakash, A comparative study to evaluate the corrosion performance of Zr incorporated Cr3C2-(NiCr) coating at 900°C. *Ceram. Int.* 44, 6479 https://doi.org/10.1016/j.ceramint.2018.01.047 (2018).

12. M. Schütze, M. Malessa, V. Rohr, and T. Weber, Development of coatings for protection in specific high temperature environments. *Surf. Coat. Technol.* 201(7), 3872 (2006).

13. J. Stringer, Coatings in the electricity supply industry: past, present, and opportunities for the future. *Surf. Coat. Technol.* 10(108), 1 (1998).

14. R.A. Mahesh, R. Jayaganthan, S. Prakash, R.A. Mahesh, R. Jayaganthan, and S. Prakash, High temperature oxidation studies on HVOF sprayed NiCrAl coatings on superalloys. *Surf. Eng.* https://doi.org/10.1179/174329409X409486 (2011).

15. G. Singh, N. Bala, and V. Chawla, High temperature oxidation behaviour of HVOF thermally sprayed NiCrAlY coating on T-91 boiler tube steel. *Mater. Today Proc.* 4, 5259 https://doi.org/10.1016/j.matpr.2017.05.035 (2017).

16. G. Biava, I.B. Siqueira, R.F. Vaz, G.B. de Souza, H.C. Jambo, A. Szogyenyi, and A.G. Pukasiewicz, Evaluation of high temperature corrosion resistance of CrN, AlCrN, and TiAlN arc evaporation PVD coatings deposited on Waspaloy. *Surf. Coat. Technol.* 25(438), 128398 https://doi.org/10.1016/j.surfcoat.2022.128398 (2022).

17. S. Wang, Y. Wang, G. Cao, C. Chen, Y. Zhu, M. Serdechnova, C. Blawert, M.L. Zheludkevich, Y. Zou, J. Ouyang, D. Jia, and Y. Zhou, High temperature oxidation and hot corrosion behaviors of PEO and PEO / polysilazane preceramic-based dual-layer coatings on Ti6Al4V alloy. *Corros. Sci.* 216, 111076 https://doi.org/10.1016/j.corsci.2023.111076 (2023).

18. C. Republic, C. Republic, Hot Corrosion Behavior of TWAS and HVOF NiCr-Based, (2023).

19. J. Cheng, Y. Wu, L. Chen, S. Hong, and L. Qiao, Hot corrosion behavior and mechanism of high-velocity arc-sprayed Ni-Cr alloy coatings. *J. Therm. Spray Technol.* 28, 1263 https://doi.org/10.1007/s11666-019-00890-0 (2019).

20. D. Meadowcroft, High temperature corrosion of alloys and coatings in oil- and coal-fired boilers. *Mater. Sci. Eng.* 88, 313 (1987).

21. B. Somasundaram, R. Kadoli, and M.R. Ramesh, Evaluation of cyclic oxidation and hot corrosion behavior of HVOF-sprayed WC-Co/NiCrAlY coating. *J. Therm. Spray Technol.* 23, 1000 https://doi.org/10.1007/s11666-014-0112-3 (2014).

22. H.S. Sidhu, B.S. Sidhu, and S. Prakash, Comparative characteristic and erosion behavior of NiCr coatings deposited by various high-velocity oxyfuel spray processes. *J. Mater. Eng. Perform.* 15, 699 https://doi.org/10.1361/105994906X150713 (2006).

23. L. Goyal, V. Chawla, and J.S. Hundal, Elevated temperature corrosion studies of AlCrN and TiAlN coatings by PAPVD on T91 boiler steel. *J. Mater. Eng. Perform.* 26, 5481 https://doi.org/10.1007/s11665-017-2972-4 (2017).

24. M.E. Aalamialeagha, S.J. Harris, and M. Emamighomi, Influence of the HVOF spraying process on the microstructure and corrosion behaviour of Ni-20%Cr coatings. *J. Mater. Sci.* 38, 4587 https://doi.org/10.1023/A:1027302122749 (2003).

25. G.R. Heath, P. Heimgartner, G. Irons, R. Miller, and S. Gustafsson, An assessment of thermal spray coating technologies for high temperature corrosion protection. *Mater. Sci. Forum* 251–254, 809 https://doi.org/10.4028/www.scientific.net/msf.251-254.809 (1997).

26. B.S. Sidhu and S. Prakash, Evaluation of the corrosion behaviour of plasma-sprayed Ni 3 Al coatings on steel in oxidation and molten salt environments at 900 8 C. *Surf. Coatings Technol.* 166, 89 (2003).

27. J.R. Nicholls, Designing oxidation-resistant coatings. *JoM.* 52(1), 28 (2000).

28. T. Sahraoui, N.E. Fenineche, G. Montavon, and C. Coddet, Structure and wear behaviour of HVOF sprayed Cr3C2-NiCr and WC-Co coatings. *Mater. Des.* 24, 309 https://doi.org/10.1016/S0261-3069(03)00059-1 (2003).

29. T.S. Sidhu, S. Prakash, and R.D. Agrawal, Characterisations of HVOF sprayed NiCrBSi coatings on Ni- and Fe-based superalloys and evaluation of cyclic oxidation behaviour of some Ni-based superalloys in molten salt environment. *Thin Solid Films* 515, 95 https://doi.org/10.1016/j.tsf.2005.12.041 (2006).

30. J.M. Miguel, J.M. Guilemany, and S. Vizcaino, Tribological study of NiCrBSi coating obtained by different processes. *Tribol. Int.* 36, 181 https://doi.org/10.1016/S0301-679X(02)00144-5 (2003).

31. Z. Liu and W. Gao, Oxidation behaviour of microcrystalline Ni-Cr-Al alloy coatings at 900°C. *Scr. Mater.* 38, 877 https://doi.org/10.1016/S1359-6462(97)00576-9 (1998).

32. G. Chen and H. Lou, Oxidation behavior of sputtered Ni-Cr-Al-Ti nanocrystalline coating. *Surf. Coat. Technol.* 123, 92 https://doi.org/10.1016/S0257-8972(99)00470-3 (2000).

33. X. Huo, J.S. Zhang, B.L. Wang, F.J. Wu, and Y.F. Han, Evaluation of NiCrAlYSi overlay coating on Ni3Al based alloy IC-6 after an engine test. *Surf. Coat. Technol.* 114, 174 https://doi.org/10.1016/S0257-8972(99)00035-3 (1999).

34. B.S. Sidhu and S. Prakash, Performance of NiCrAlY, Ni-Cr, Stellite-6 and Ni3Al coatings in Na2SO4-60% V2O5environronment at 900°C under cyclic conditions. *Surf. Coat. Technol.* https://doi.org/10.1016/j.surfcoat.2006.02.035 (2006).

35. P. Niranatlumpong, and H. Koiprasert, The effect of Mo content in plasma-sprayed Mo-NiCrBSi coating on the tribological behavior. *Surf. Coat. Technol.* 205, 483 https://doi.org/10.1016/j.surfcoat.2010.07.017 (2010).

36. J. Lee, P. Tsai, and J. Lee, Cyclic oxidation behavior and microstructure evolution of aluminized. *Pt-alum. High Velocity Oxygen Fuel Sprayed. CoNiCrAlY Coat.* 517, 5253 https://doi.org/10.1016/j.tsf.2009.03.148 (2009).

37. W. Brandl, D. Toma, and H.J. Grabke, The characteristics of alumina scales formed on HVOF-sprayed MCrAlY coatings. *Surf. Coat. Technol.* 108–109, 10 https://doi.org/10.1016/S0257-8972(98)00613-6 (1998).

38. G.A. Kolta, I.F. Hewaidy, and N.S. Felix, Reactions between sodium sulphate and vanadium pentoxide. *Thermochim. Acta* 4, 151 https://doi.org/10.1016/s0040-6031(72)80029-7 (1972).

39. Y.S. Zhang, M. Takemoto, R.A. Rapp, Hot corrosion of nickel-chromium and nickel-chromium-aluminum thermal-spray coatings by sodium sulfate-sodium metavanadate salt, Corros. Sci. 680–689 (1996).

40. Y.S. Hwang and R.A. Rapp, Thermochemistry and solubilities of oxides in sodium sulfate-vanadate solutions. *Corrosion* 45(11), 933 (1989).

41. V. Lakkannavar, K.B. Yogesha, C.D. Prasad, M. Mruthunjaya, and R. Suresh, A review on tribological and corrosion behaviour of thermal spray coatings. *J. Inst. Eng. India.* https://doi.org/10.1007/s40033-024-00636-5 (2024).

42. H. Nayak, S. Kollur, K. Prasad, C. Suresh Erannagari, D. Prasad, and N. Nagabhushana, Development of equal proportional YSZ+Al$_2$O$_3$ thermal barrier coating and effect of coating thickness on the corrosion behaviour on cast iron substrate. *High Temp. Corros. Mater. Springer.* https://doi.org/10.1007/s11085-024-10222-5 (2024).

43. C.D. Prasad, S. Kollur, C.R. Aprameya, T.V. Chandramouli, T. Jagadeesha, and B.N. Prashanth, Investigations on tribological and microstructure characteristics of WC-12Co/FeNiCrMo composite coating by HVOF process. *JOM* 76(1), 186 https://doi.org/10.1007/s11837-023-06242-2 (2024).

44. G. Madhu Sudana Reddy, C. Durga Prasad, S. Kollur, A. Lakshmikanthan, R. Suresh Kumar, and C.R. Aprameya, Investigation of high-temperature erosion behavior of Ni-CrAlY/TiO2 plasma coatings on titanium substrate. *JOM* 75(9), 3317 (2023).

45. C.D. Prasad, S. Kollur, M. Nusrathulla, G. Satheesh Babu, M.B. Hanamantraygouda, B.N. Prashanth, and N. Nagabhushana, Characterisation and wear behaviour of SiC reinforced FeNiCrMo composite coating by HVOF process. *Trans. IMF.* 102(1), 22 (2024).

46. G.M. Reddy, C.D. Prasad, P. Patil, G. Shetty, N. Kakur, and M.R. Ramesh, High temperature erosion performance of NiCrAlY/Cr$_2$O$_3$/YSZ plasma spray coatings. *Trans. IMF.* 101(5), 245 https://doi.org/10.1080/00202967.2023.2208899 (2023).

47. H. Sharanabasava, C.D. Prasad, and M.R. Ramesh, Characterization and wear behavior of NiCrMoSiC microwave cladding. *J. Mater. Eng. Perform.* 33(2), 763 (2024).

48. G.M. Reddy, C.D. Prasad, P. Patil, N. Kakur, and M.R. Ramesh, Investigation of plasma sprayed NiCrAlY/Cr$_2$O$_3$/YSZ coatings on erosion performance of MDN 420 steel substrate at elevated temperatures. *Int. J. Surf. Sci. Eng.* 17(3), 180 https://doi.org/10.1504/IJSURFSE.2023.10054266 (2023).

49. H. Sharanabasava, C.D. Prasad, and M.R. Ramesh, Effect of Mo-and SiC-reinforced NiCr microwave cladding on microstructure, mechanical and wear properties. *J. Inst. Eng. India.* 104(2), 539 https://doi.org/10.1007/s40033-022-00445-8 (2023).

50. G.M. Reddy, C.D. Prasad, P. Patil, G. Shetty, M.R. Ramesh, and T.N. Rao, Investigation of thermally sprayed NiCrAlY/TiO$_2$ and NiCrAlY/Cr$_2$O$_3$/YSZ cermet composite coatings on titanium alloys. *Eng. Res. Express.* 4(2), 025049 https://doi.org/10.1088/2631-8695/ac7946 (2022).

51. H.S. Nithin, K.M. Nishchitha, D.G. Pradeep, C.P. Durga, and M. Mathapati, Comparative analysis of CoCrAlY coat-

ings at high-temperature oxidation behavior using different reinforcement composition profiles. *Welding World.* 67(3), 585 https://doi.org/10.1007/s40194-022-01405-2 (2023).

52. C.D. Prasad, P. Patil, N. Kakur, and M.R. Ramesh, Elevated temperature erosion performance of plasma sprayed Ni-CrAlY/TiO$_2$ coating on MDN 420 steel substrate. *Surf. Topogr. Metrol. Prop.* 10(2), 025010 https://doi.org/10.1088/2051-672X/ac6a6e (2022).

53. G.M. Reddy, C.D. Prasad, G. Shetty, M.R. Ramesh, T.N. Rao, and P. Patil, High-temperature oxidation behavior of plasma-sprayed NiCrAlY/TiO2 and NiCrAlY/Cr2O3/YSZ coatings on titanium alloy. *Welding World.* https://doi.org/10.1007/s40194-022-01268-7 (2022).

54. T. Naik, C. Mahantayya Mathapathi, D. Prasad, H.S. Nithin, and M.R. Ramesh, Effect of laser post treatment on microstructural and sliding wear behavior of HVOF sprayed NiCrC and NiCrSi coatings. *Surf. Rev. Lett.* 29(1), 225000 https://doi.org/10.1142/S0218625X2250007X (2022).

55. G.M. Reddy, C.D. Prasad, G. Shetty, M.R. Ramesh, T.N. Rao, and P. Patil, High temperature oxidation studies of plasma sprayed NiCrAlY/TiO2 & NiCrAlY/Cr2O3/YSZ cermet composite coatings on MDN-420 special steel alloy. *Metallogr. Microstruct. Anal.* 10, 642 https://doi.org/10.1007/s13632-021-00784-0 (2021).

56. G. Madhu, K.M. Mrityunjaya Swamy, D.A. Kumar, C.D. Prasad, and U. Harish, Evaluation of hot corrosion behavior of HVOF thermally sprayed Cr$_3$C$_2$ -35NiCr coating on SS 304 boiler tube steel. *Am. Inst. Phys.* 2316, 030014 https://doi.org/10.1063/5.0038279 (2021).

57. C. Durga Prasad, M.R. Akhil Jerri, and Ramesh, Characterization and sliding wear behavior of iron based metallic coating deposited by HVOF process on low carbon steel substrate. *J. Bio Tribo-Corros. Springer* 6, 69 https://doi.org/10.1007/s40735-020-00366-7 (2020).

58. M.S. Reddy, C. Durga Prasad, M.R. Pradeep Patil, and N.R. Ramesh, Hot corrosion behavior of plasma sprayed Ni-CrAlY/TiO$_2$ and NiCrAlY/Cr$_2$O$_3$/YSZ cermets coatings on alloy steel. *Surf. Interfaces Elsevier Sci.* 22, 100810 https://doi.org/10.1016/j.surfin.2020.100810 (2021).

59. A.R. Kannan, V. Rajkumar, C.D. Prasad, N.S. Shanmugam, and J. Yoon, Microstructure and hot corrosion performance of stainless steel 347 produced by wire arc additive manufacturing. *Vacuum* 1(210), 111901 https://doi.org/10.1016/j.vacuum.2023.111901 (2023).

60. C.D. Prasad, S. Joladarashi, M.R. Ramesh, and M.S. Srinath, Microstructural and tribological resistance of flame-sprayed CoMoCrSi/WC-CrC-Ni and CoMoCrSi/WC-12Co composite coatings remelted by microwave energy. *J. Bio Tribo Corros.* 6, 1 https://doi.org/10.1007/s40735-020-00421-3 (2020).

61. C. Durga Prasad, and M.R. Sharnappa Joladarashi Ramesh, Comparative investigation of HVOF and flame sprayed Co-MoCrSi coating. *Am. Inst. Phys.* 2247, 050004 https://doi.org/10.1063/5.0003883 (2020).

62. C.D. Prasad, S. Joladarashi, M.R. Ramesh, M.S. Srinath, and B.H. Channabasappa, Comparison of high temperature wear behavior of microwave assisted HVOF sprayed Co-MoCrSi-WC-CrC-Ni/WC-12Co composite coatings. *SILICON* 12, 3027 https://doi.org/10.1007/s12633-020-00398-1 (2020).

63. A.R. Kannan, C.D. Prasad, V. Rajkumar, N.S. Shanmugam, W. Lee, and J. Yoon, Hot oxidation and corrosion behaviour of boiler steel fabricated by wire arc additive manufacturing. *Mater Charact* 1(203), 113113 https://doi.org/10.1016/j.matchar.2023.113113 (2023).

64. C. Durga Prasad, M.R. Sharnappa Joladarashi, M.S. Ramesh, B.H. Srinath, and Channabasappa., Effect of microwave heating on microstructure and elevated temperature adhesive wear behavior of HVOF deposited CoMoCrSi-Cr$_3$C$_2$ composite coating. *Surf. Coat. Technol. Elsevier Sci.* 374, 291 https://doi.org/10.1016/j.surfcoat.2019.05.056 (2019).

65. K.G. Girisha, C. Durga Prasad, K.C. Anil, and K.V. Sreenivas Rao, Dry sliding wear behaviour of Al2O3 coat-

ings for AISI 410 grade stainless steel. *Appl. Mech. Mater.* 5(766), 585 https://doi.org/10.4028/www.scientific.net/AMM. 766-767.585 (2015).

66. C. Durga Prasad, M.R. Sharnappa Joladarashi, M.S. Ramesh, B.H. Srinath, and Channabasappa, Development and sliding wear behavior of Co-Mo-Cr-Si cladding through microwave heating. *Silicon Springer* 11, 2975 https://doi.org/10.1007/s12633-019-0084-5 (2019).

67. C. Durga Prasad, M.R. Sharnappa Joladarashi, M.S. Ramesh, B.H. Srinath, and Channabasappa., Microstructure and tribological behavior of flame sprayed and microwave fused CoMoCrSi/CoMoCrSi-$Cr_3C_2$ coatings. *Mater. Res. Express IOP* 6, 026512 https://doi.org/10.1088/2053-1591/aaebd9 (2019).

68. C. Durga Prasad, M.R. Sharnappa Joladarashi, M.S. Ramesh, B.H. Srinath, and Channabasappa., Influence of microwave hybrid heating on the sliding wear behaviour of HVOF sprayed CoMoCrSi coating. *Mater. Res. Express IOP* 5, 086519 https://doi.org/10.1088/2053-1591/aad44e (2018).

69. K.G. Girisha, K.V. Sreenivas Rao, and C. Durga Prasad, Slurry erosion resistance of martenistic stainless steel with plasma sprayed $Al_2O_3$-40%$TiO_2$ coatings. *Mater. Today Proceed.* 5, 7388 https://doi.org/10.1016/j.matpr.2017.11.409 (2018).

70. C. Durga Prasad, M.R. Sharnappa Joladarashi, and A.S. Ramesh, High temperature gradient cobalt based clad developed using microwave hybrid heating. *Am. Inst. Phys.* 1943, 020111 https://doi.org/10.1063/1.5029687 (2018).

71. K.G. Girisha, R. Rakesh, C. Durga Prasad, and K.V. Sreenivas Rao, Development of corrosion resistance coating for AISI 410 grade steel. *Appl. Mech. Mater.* 813–814, 135 https://doi.org/10.4028/www.scientific.net/AMM.813-814.135 (2015).